Calculation of a Three-Dimensional Shock Wave-Turbulent Boundary-Layer Interaction

L. Cambier* and B. Escande†
Office National d'Etudes et de Recherches Aérospatiales, BP 72-92322 Châtillon Cedex, France

This paper deals with the numerical simulation of a shock wave-turbulent boundary-layer interaction in a three-dimensional channel by solution of the Reynolds averaged Navier-Stokes equations with a mixing-length turbulence model. The numerical method is characterized by an explicit centered finite-difference scheme associated with a multigrid convergence acceleration. The computed configuration is well suited to the validation of a three-dimensional Navier-Stokes solver since the flow has a very complex three-dimensional structure, although the channel geometry is simple. Comparison with experiment shows that the numerical results obtained in a mesh containing about 600,000 points are satisfactory.

Introduction

TRANSONIC shock wave-turbulent boundary-layer interactions represent one of the main problems in fluid mechanics because of the occurrence of such interactions in a variety of applications (including both external and internal flows) and because of their significant influence on performance. Important examples include the interactions occurring on wings in transonic flight that induce harmful effects such as drag rise as well as the interactions occurring in compressors that can lead to considerable performance losses.

The prediction of shock wave-turbulent boundary-layer interactions is therefore of great practical interest. For the sake of simplicity, much of the effort in the past has obviously focused on understanding the two-dimensional case. At Office National d'Etudes et de Recherches Aérospatiales, numerical results were obtained by solving the Navier-Stokes equations for two-dimensional interactions and compared[1,2] with measurements[3] also performed at ONERA.

In practice, however, most of the interaction flows are strongly three-dimensional and often incorporate large gradients of flow quantities in each of the three space directions. Nowadays, the capacity of the available supercomputers allows the tackling of this type of problem by solving the three-dimensional Reynolds averaged Navier-Stokes equations. Nevertheless, the quality of the numerical results strongly depends on the turbulence modeling and on the mesh fineness. The validity of a computational method must therefore be carefully established by means of detailed comparisons with reliable experimental data.

This paper presents the results obtained with a new three-dimensional Navier-Stokes solver for the computation of a complex shock wave-turbulent boundary-layer interaction in a transonic channel. The three-dimensional Navier-Stokes solver has been built up from a three-dimensional Euler solver[4] and a two-dimensional Navier-Stokes solver,[5] both developed at ONERA. The numerical method is characterized by an explicit centered finite-difference scheme associated with a multigrid convergence acceleration. The three-dimensional Navier-Stokes solver has been applied to a configuration defined and studied experimentally at ONERA.[6] The detailed set of available experimental data has allowed the evaluation of the quality of the numerical results.

Received April 19, 1989; presented as Paper 89-1851 at the AIAA 20th Fluid Dynamics, Plasma Dynamics, and Laser Conference, June 12-14, 1989; revision received Dec. 27, 1989; accepted for publication Dec. 28, 1989.

*Research Scientist, Aerodynamics Department.
†Research Scientist, Energetics Department.

Analysis

Flow Governing Equations

The theoretical model for this study is the compressible Reynolds-averaged Navier-Stokes equations associated with an algebraic mixing-length type turbulence model.

The Navier-Stokes equations for describing the mean flow are written in the following compact form:

$$\frac{\partial f}{\partial t} + \operatorname{div}(F - F_v) = 0 \tag{1}$$

where $f = (\rho, \rho\bar{V}, \rho E)$ denotes the unknowns, and the flux densities $F = (\rho\bar{V},\ \rho\bar{V}\times\bar{V} + p\bar{\bar{I}},\ \rho E\bar{V} + p\bar{V})$ and $F_v = (0, \bar{\bar{\tau}} + \bar{\bar{\tau}}_R, (\bar{\bar{\tau}} + \bar{\bar{\tau}}_R)\bar{V} - \bar{q} - \bar{q}_t)$ represent the inviscid fluid terms and the dissipative terms, respectively.

In the expression for f, ρ, V, and E denote the density, the flow velocity, and the total energy per unit mass, respectively.

The equation of state for a perfect gas with constant specific heats in a ratio $C_p/C_v = \gamma$ relates the static pressure p to ρ, V and E by

$$p = (\gamma - 1)\rho\left(E - \frac{V^2}{2}\right) \tag{2}$$

A Newtonian fluid verifying Stokes' hypothesis is considered, and the equations for the stress tensor $\bar{\bar{\tau}}$ and the heat flux density vector $\bar{q}$ are written

$$\bar{\bar{\tau}} = -\frac{2}{3}\mu \operatorname{div} \bar{V}\bar{\bar{I}} + \mu[\nabla\bar{V} + \nabla\bar{V}^T]$$

$$\bar{q} = -\mathrm{X}\nabla T \tag{3}$$

where μ is the coefficient of viscosity, which varies as a function of the static temperature T according to Sutherland's law, and X is the coefficient of heat conductibility given by $\mathrm{X} = \mu C_p/P_r$. (The Prandtl number Pr is assumed to be constant and equal to 0.72.)

The expressions for the Reynolds stress tensor $\bar{\bar{\tau}}_R$ and the enthalpy turbulent diffusion flux density vector q_t are given by the turbulence model. The results presented in this paper have been obtained with an algebraic turbulence model, which has been chosen for simplicity sake in a first numerical investigation of a very complex flowfield. The tensor $\bar{\bar{\tau}}_R$ and the vector

$\bar{q}_t$ are then related to the velocity gradient and the temperature gradient by expressions analogous to Eq. (3), i.e.,

$$\bar{\bar{\tau}}_R = -\frac{2}{3}\mu_t \operatorname{div} \bar{V}\bar{\bar{I}} + \mu_t [\nabla \bar{V} + \nabla \bar{V}^T]$$

$$\bar{q}_t = -\frac{\mu_t C_p}{Pr_t} \nabla T \tag{4}$$

The turbulent Prandtl number Pr_t is assumed to be constant and equal to 0.9, and the modeling of the turbulence then comes down to evaluating the eddy viscosity coefficient μ_t. To do this, we have used a mixing-length model initially developed by Michel, Quémard, and Durant[7] within the framework of the boundary-layer approximation and for two-dimensional flows. This model is an inexpensive one-layer model that we have already used for two-dimensional Navier-Stokes calculations.[1,2,5] We are now going to discuss the implementation of this turbulence model in the three-dimensional Navier-Stokes equation case.

Turbulence Model Implementation

The eddy viscosity coefficient is given by

$$\mu_t = \rho \ell^2 F^2 |\bar{\Omega}| \tag{5}$$

where $\bar{\Omega}$ denotes the vorticity ($\bar{\Omega} = curl\ \bar{V}$), ℓ is the mixing length, and F is the viscous sublayer damping function.

The normal derivative of the tangential velocity component used in the original model[7] for the boundary-layer equation case is replaced in Eq. (5) by the magnitude $|\bar{\Omega}|$ of the vorticity.

The mixing length ℓ is given by

$$\ell = 0.085\ \delta \tanh\left(\frac{Kd}{0.085\delta}\right), \qquad (K = 0.41) \tag{6}$$

where d denotes Buleev's "modified distance[8]" and δ is a "modified boundary-layer thickness.[9]" The determination of d and δ will be described below.

The damping function F is given by

$$F(\zeta) = 1. - \exp\left(-\frac{\sqrt{\zeta}}{26K}\right), \qquad \zeta = \rho \ell^2 \frac{\mu + \mu_t}{\mu^2} |\bar{\Omega}| \tag{7}$$

It will be noted that the definition of the intermediate variable ζ involves the coefficient μ_t and that, consequently, to determine μ_t by Eq. (5), an implicit equation has to be solved. In practice, this equation is solved by a fixed-point method.

A modified distance d is used to account for the turbulent length scale corresponding to the influence of several walls (when there is only one wall, d is equal to the normal distance from the wall). In the present study, turbulence is under the influence of four walls. For a channel with a rectangular cross section, the expression for the modified distance d at point M is:[8]

$$d = \frac{2y_1z_1y_2z_2}{y_2z_2\sqrt{y_1^2+z_1^2} + y_1z_2\sqrt{z_1^2+y_2^2} + y_2z_1\sqrt{y_1^2+z_2^2} + y_1z_1\sqrt{y_2^2+z_2^2}} \tag{8}$$

where y_1 and y_2 are the distances of M from two opposite sides of the section, and z_1 and z_2 are the distances of M from the other two sides. Although the cross section of our channel is not exactly rectangular everywhere, we have still used Eq. (8).

The values of the modified boundary-layer thickness δ are determined from the values of d at the edge of the boundary-layer.[9] More precisely, in each mesh plane (Y,Z), where the coordinates Y and Z correspond to the indices of the discretization points (see Fig. 1), the edge of the boundary-layer is searched for towards the four corners. It is defined as the

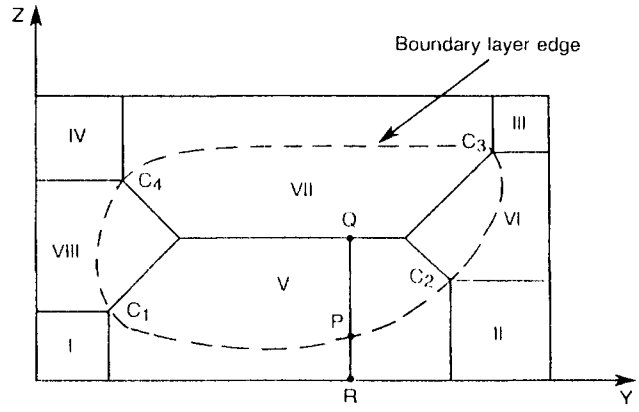

Fig. 1 Sketch of boundary-layer thickness determination.

points C_1, C_2, C_3, and C_4 of the four bisectors where the magnitude $|\bar{\Omega}|$ of the vorticity is more than some value Ω_0. The (Y,Z) plane is then divided into eight regions, as shown in Fig. 1. In the corner regions I, II, III, and IV, the value of δ is treated as a constant in each region, respectively equal to the value of d at points C_1, C_2, C_3, and C_4. In the region V, along each mesh line $Y = Const$ and towards the wall, the edge of the boundary-layer (for example, point P) is located where $|\bar{\Omega}|$ is more than Ω_0; the value of δ on segment QR (see Fig. 1) is constant and equal to the value of d at P. Regions VI, VII, and VIII are treated in a way similar to region V.

Numerical Method

The numerical method is characterized by an explicit-centered finite-difference scheme associated with a multigrid convergence acceleration; it is derived from the method presented by Vuillot[4] for the three-dimensional Euler equations and by Cambier, Couaillier, and Veuillot[5] for the two-dimensional Navier-Stokes equations.

Numerical Scheme

Equation (1) is discretized using a two-step Lax-Wendroff-type scheme; the dissipative terms are taken into account according to Thommen's idea.[10]

The solution f^{n+1} at time $t^{n+1} = t^n + \Delta t$ is given by the following two steps:

$$f^{n+1/2} = f^n - \frac{\Delta t}{2} \operatorname{div}(F^n - F_v^n) \tag{9a}$$

$$f^{n+1} = f^n - \Delta t \operatorname{div}(F^{n+1/2} - F_v^n) \tag{9b}$$

The space discretization of both divergence terms, div $(F^n - F_v^n)$ in the first step [Eq. (9a)] and div $(F^{n+1/2} - F_v^n)$ in the second step [Eq. (9b)] is performed using the contour integral formula

$$\operatorname{div}\phi = \frac{1}{v(\omega)} \int_{\partial\omega} \phi \bar{n}\, dS \tag{10}$$

In the predictor step, the control volumes ω are cells of the basic mesh and divϕ (with $\phi = F^n - F_v^n$) is obtained at the centers of these cells. In the second step, the control volumes ω are the cells of a staggered mesh, the nodes of which are the cell centers of the basic mesh and divϕ (with $\phi = F^{n+1/2} - F_v^n$) is obtained at the nodes of the basic mesh. The computation of the contour integral $\int_{\partial\omega} \phi\, \bar{n}\, dS$ in Eq. (10) is detailed in Ref. 4.

The dissipative terms F_v are calculated using central difference formulas and are stored at the mesh points. More precisely, the velocity gradient $\nabla \bar{V}$ and the temperature gradient ∇T at a mesh point M of indices (i,j,k) are evaluated by the following contour integral formulas:

$$\nabla \bar{V} = \frac{1}{v(\omega)} \int_{\partial\omega} \bar{V} \times \bar{n}\, dS$$
$$\nabla T = \frac{1}{v(\omega)} \int_{\partial\omega} T\bar{n}\, dS \tag{11}$$

where the volume ω is the cell of the staggered mesh, which contains M and is defined by indices denoted $(i \pm \frac{1}{2}, j \pm \frac{1}{2}, k \pm \frac{1}{2})$. The contour integrals of Eq. (11) are evaluated by assuming that $\bar{V}$ and T are constant on each of the eight sides of the volume ω [for instance the $(k - \frac{1}{2})$ side in Fig. 2] and are calculated as the half-sum of the values of $\bar{V}$ and T at the two neighboring nodes of the basic mesh (points M and P in Fig. 2).

Two artificial viscosity terms[4] consisting of a second-order nonlinear term and a fourth-order linear term are added to improve the stability properties of the scheme and to correctly capture the flow discontinuities in the inviscid flow regions.

The local time step used in the computations is determined from the following formula that takes into account the CFL and diffusion limitations:

$$\Delta t = \eta \,\text{Min}\left[\frac{h}{V + a}, \frac{\rho h^2}{2\gamma\left(\frac{\mu}{Pr} + \frac{\mu_t}{Pr_t}\right)}\right] \tag{12}$$

where a denotes the speed of sound, η is a numerical coefficient of the order of unity introduced because of the approximate character of the criterion, and h is a characteristic length of the mesh size.

Multigrid Acceleration Technique

To accelerate the convergence towards a steady flow solution, a multigrid acceleration technique has been applied. This technique is based on the multigrid scheme presented by Ni for the two-dimensional Euler equations[11] and was successively applied at ONERA in the two-dimensional Euler equation case,[12] in the two-dimensional Navier-Stokes equation case,[5] and in the three-dimensional Euler equation case.[13]

In comparison with Ni's method, some time advance coefficients have been introduced and optimized according to a Fourier analysis carried out in the case of a one-dimensional transport equation.[14]

The multigrid acceleration applied to Eq. (1) consists of integrating on coarse grids a residual system based on the time derivation of the inviscid equations only. Thus, we use the multigrid phase developed for the three-dimensional Euler equations without modifying it.

The three-dimensional Navier-Stokes calculation described here has been carried out using two coarse grids in the multigrid phase. The values of the time advance coefficients α_k and β_k (defined for example in Ref. 5) were $\alpha_k = 1$, and $\beta_k = 2^k$.

Results and Discussion

Description of the Configuration

The previously described Navier-Stokes solution procedure has been applied to a configuration of a shock wave-turbulent boundary-layer interaction in a three-dimensional transonic channel. This configuration has been defined at ONERA and tested experimentally in the ONERA S8 wind tunnel at Chalais-Meudon. The experimental analysis of the flow was carried out by Benay, Délery, and Pot.[6]

The geometry of the channel shown in Fig. 3 consists of three flat walls and a humped lower wall. The upstream part of the hump is a ramp, inclined approximately 7 deg from a horizontal plane. This ramp is followed by a convex circular surface and a concave circular surface defined so as to ensure slope continuity everywhere. The angle formed by the hump crest line and the channel axis is equal to 60 deg. The maximum height of the hump is 20 mm, whereas the channel section is 120 mm wide and 100 mm high at the inlet.

This configuration is well suited to the validation of a computation code. Indeed, although the very smooth channel geometry has been defined to make it easy to discretize by a numerical mesh, the flow generated with this geometry has a very interesting complex three-dimensional structure.

The stagnation conditions in the experiment are the following: stagnation pressure $p_{t_0} = 92{,}000$ Pa and stagnation temperature $T_{t_0} = 290$ K. The Reynolds number based on the stagnation conditions and on the inlet section height $H = 100$ mm is equal to $2.027\ 10^6$.

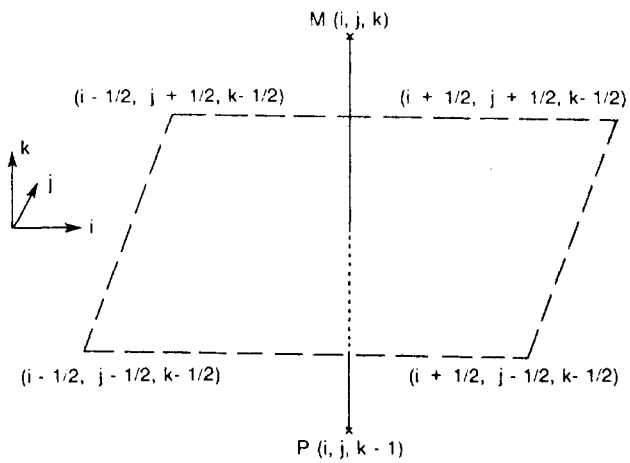

Fig. 2 Sketch of dissipative term evaluation.

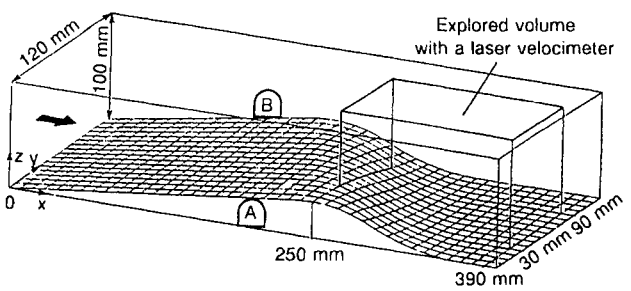

Fig. 3 Definition of the transonic channel.[6]

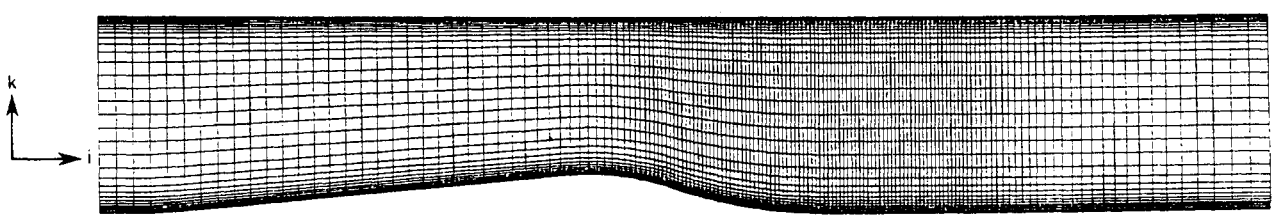

Fig. 4 (153×61) mesh in a j-plane.

Computational Domain and Boundary Conditions

The computational domain extends from $x = -30$ mm to $x = 560$ mm, whereas the hump, starting at $x = 0$ mm, stretches to $x = 370$ mm on side A (see Fig. 3).

In the experiment, the shock wave position is adjusted by means of a second throat. In the computation, this position results from the value of the static pressure imposed at the downstream boundary of the domain. The static pressure value in the computation ($p_2/p_{t_0} = 0.545$) has been adjusted to give the experimental shock location at convergence. It was not possible to set up the experimental value because the static pressure had not been measured so far downstream.

In the upstream boundary of the domain, the boundary conditions applied are the values p_{t_0} and T_{t_0} of the stagnation pressure and stagnation temperature as well as the direction of the velocity, which is assumed to be parallel to the x axis. In the experiment, the upstream boundary-layer thickness is very small and does not need to be represented at this location.

At both upstream and downstream boundaries, the boundary conditions applied are complemented by characteristic relations to determine the complete set of variables. This characteristic relation technique is founded on the mathematical properties of the hyperbolic systems[15] and is also used in the framework of the Navier-Stokes equations.[5]

At the walls, a no-slip condition is applied, and the temperature is set at the stagnation temperature T_{t_0}. The static pressure is computed by assuming its derivative to be zero along the mesh line passing through the point considered and practically normal to the wall.

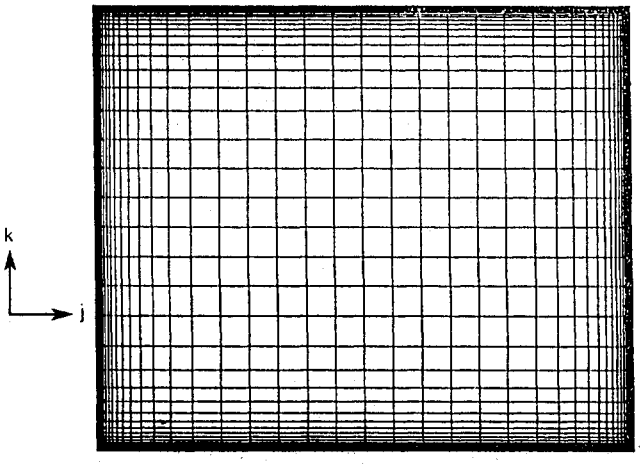

Fig. 5 (65×61) mesh in a i-plane.

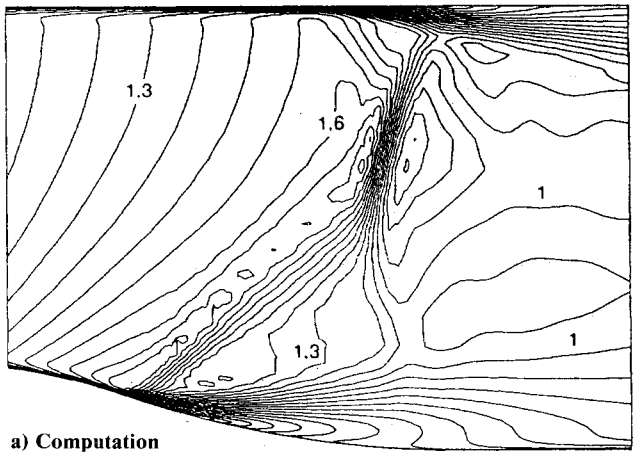

a) Computation

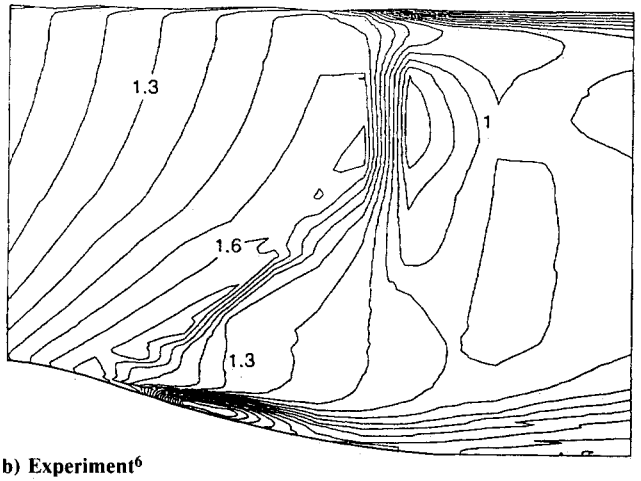

b) Experiment[6]

Fig. 7 Iso-Mach number contours in the plane $y = 30$ mm in the interaction region ($\Delta M = 0.075$).

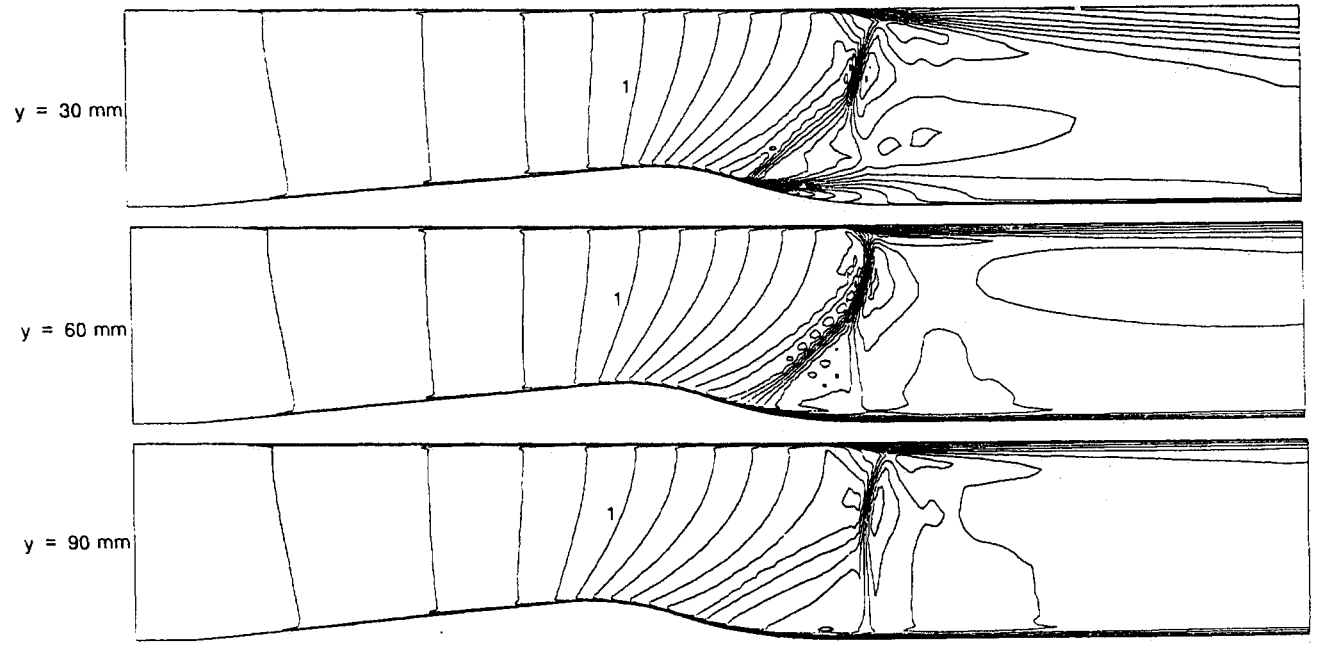

Fig. 6 Computed iso-Mach number contours ($\Delta M = 0.1$).

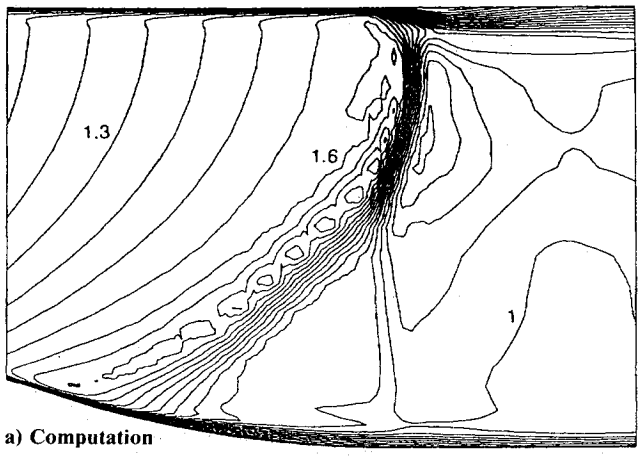

a) Computation

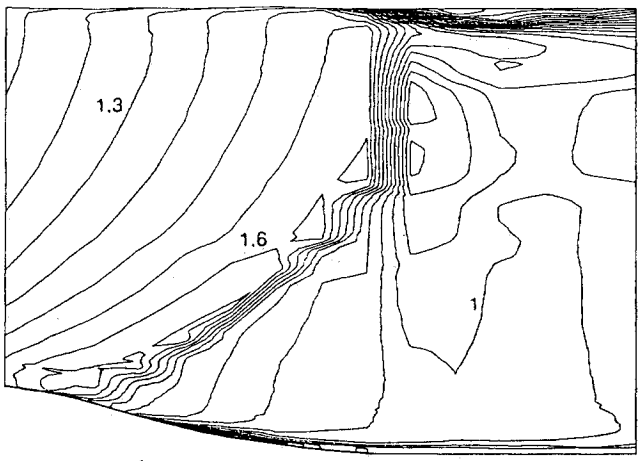

b) Experiment[6]

Fig. 8 Iso-Mach number contours in the middle plane ($y = 60$ mm) in the interaction region ($\Delta M = 0.075$).

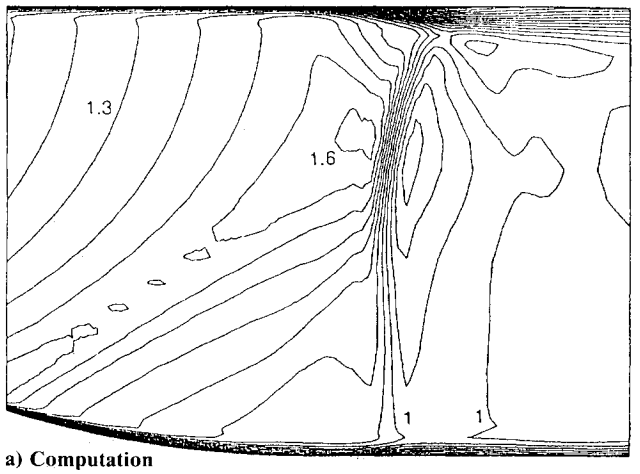

a) Computation

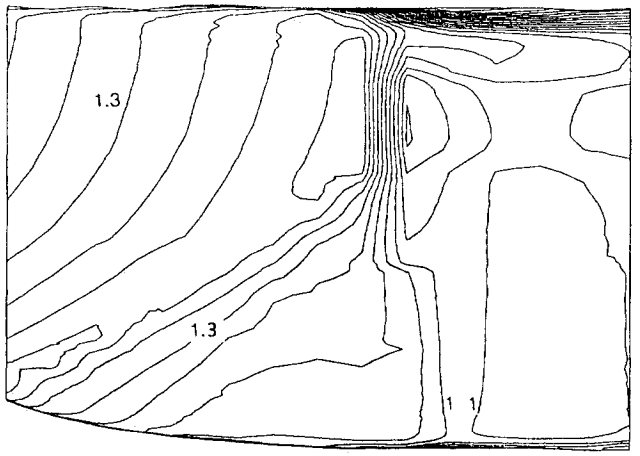

b) Experiment[6]

Fig. 9 Iso-Mach number contours in the plane $y = 90$ mm in the interaction region ($\Delta M = 0.075$).

Description of the Computation

The three families of mesh planes have been defined such that the i planes, the j planes, and the k planes correspond respectively to x planes, to y planes and to surfaces that are interpolated between the humped lower wall and the flat upper wall. Figures 4 and 5 show the mesh in a j plane and in an i plane. The number of mesh points is equal to $153 \times 65 \times 61 = 606{,}645$. The mesh is highly stretched in the j and k directions near the four walls for an adequate resolution of the viscous layers. The mesh size at the walls is equal to 0.008 mm in the j direction and 0.010 mm in the k direction, whereas the spacing in the streamwise direction in the interaction region is equal to 2 mm. At the abscissa $x = 260$ mm located just upstream of the interaction, the maximum value of the mesh spacing y^+ in dimensionless wall units is equal to 3.2 in the j direction and to 3.8 in the k direction. Thus, the first row of points adjacent to the walls is located inside the linear sublayer.

The initial conditions correspond to an inviscid one-dimensional flow with a shock located at $x = 300$ mm (approximately at the experimental position).

The computing time on a CRAY-2 is equal to about 12 s for one iteration (that is to say, 20 μs for one iteration and one mesh point). A plotting accuracy and a three-decade decrease of the residuals are obtained after 5000 iterations.

Analysis of the Numerical Results

The computed flow is first represented in Fig. 6 with the iso-Mach number contours in three planes parallel to the lateral walls and located respectively at $y = 30$ mm, $y = 60$ mm, and $y = 90$ mm. The strongly three-dimensional structure of the flow in the interaction region and downstream is clearly revealed by comparing the contours in the three planes. In particular, a lambda shock pattern on the lower wall can be observed in the first two planes whereas in the plane $y = 90$ mm, the oblique shock of the lambda is considerably weakened and nearly replaced by a continuous compression. Besides, the thickening of the lower and upper wall boundary layers is far more important in the plane $y = 30$ mm (which is the plane closest to side wall A where the hump last peaks) than in the other two planes.

Figures 7–9 show a comparison of the computed and experimental iso-Mach number contours in the interaction region in the three previously considered longitudinal planes. The experimental values[6] have been obtained by using a three-component laser velocimeter (the volume explored by the laser velocimeter is shown in Fig. 3). Considering the experimental contours, it should be noticed first that the boundary-layer is nearly invisible upstream of the shock because the velocimeter cannot operate very close to the wall, and second, that the shock thickness is due to the plotting procedure which interpolates linearly between the measurement points.

The comparison shown in Figs. 7–9 is satisfactory, especially if one takes into consideration that the mesh is probably too coarse both in the i direction in the interaction region and in the j and k directions in the center of the channel and that the turbulence modeling is inadequate to the representation of large separated regions. In particular, the computation correctly describes the evolution of the lambda shock wave structure as we move from wall A to wall B (that is to say, as y increases). The most important discrepancy between computation and experiment takes place in the plane closest to wall A,

where too strong a thickening of the boundary-layers in the interaction region is predicted by the computation.

The structure of the computed flow is also displayed by Figs. 10–12, representing the iso-Mach number contours in three transverse planes respectively located upstream of the interaction (at $x = 260$ mm), in the interaction (at $x = 300$ mm), and at the end of the interaction (at $x = 340$ mm). Figures 10–12 show the major thickening of the boundary-layers and the considerable phenomena appearing in the corners, the interpretation of which will be made easier by the plottings of velocity vectors in the transverse planes. The trace of the oblique shock wave is visible in the plane $x = 300$ mm (see Fig. 11).

Figures 13–15 show the velocity vector projections in the same three transverse planes. In the first plane (at $x = 260$ mm in Fig. 13), under the effect of the swept hump, the major portion of the transverse flow runs from face A to face B and from the upper wall to the lower wall; the transverse compo-

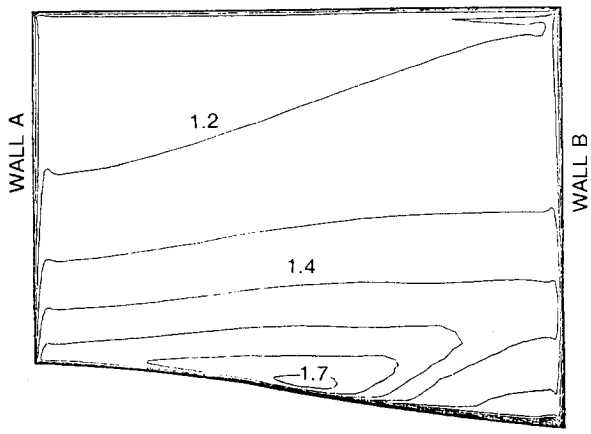

Fig. 10 Iso-Mach number contours in the transverse plane $x = 260$ mm ($\Delta M = 0.1$).

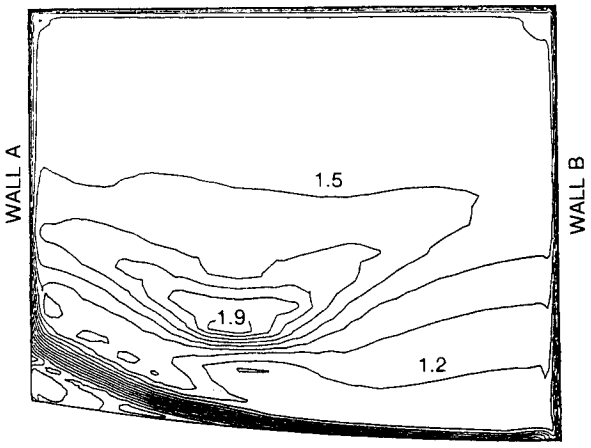

Fig. 11 Iso-Mach number contours in the transverse plane $x = 300$ mm ($\Delta M = 0.1$).

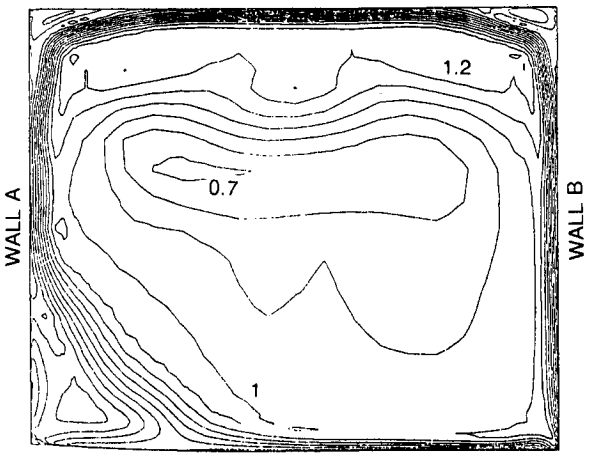

Fig. 12 Iso-Mach number contours in the transverse plane $x = 340$ mm ($\Delta M = 0.1$).

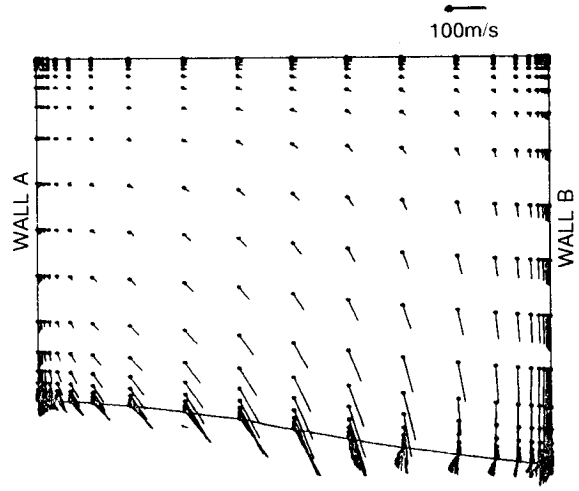

Fig. 13 Velocity vector projections in the transverse plane $x = 260$ mm (the dots correspond to the vector origins).

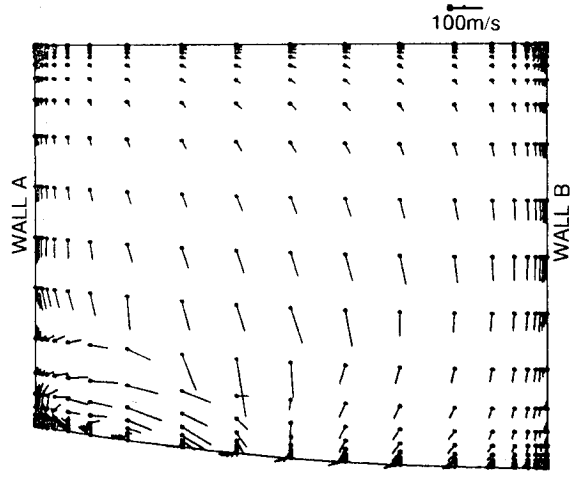

Fig. 14 Velocity vector projections in the transverse plane $x = 300$ mm.

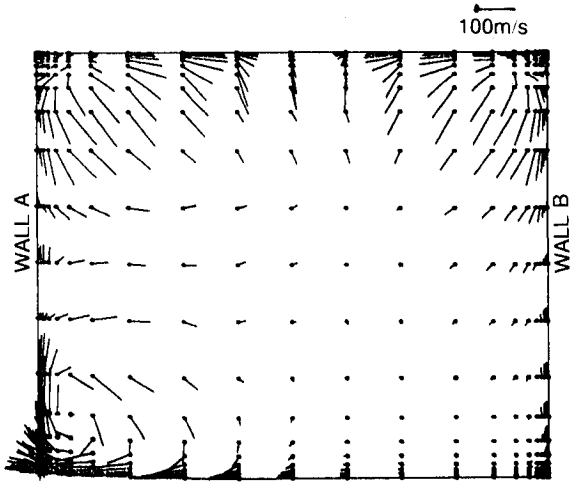

Fig. 15 Velocity vector projections in the transverse plane $x = 340$ mm.

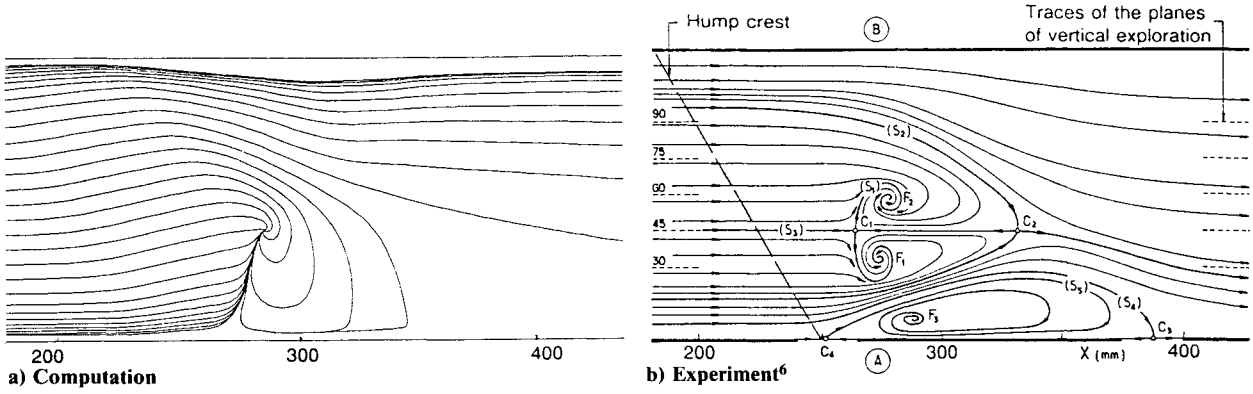

Fig. 16 Skin-friction lines on the lower wall.

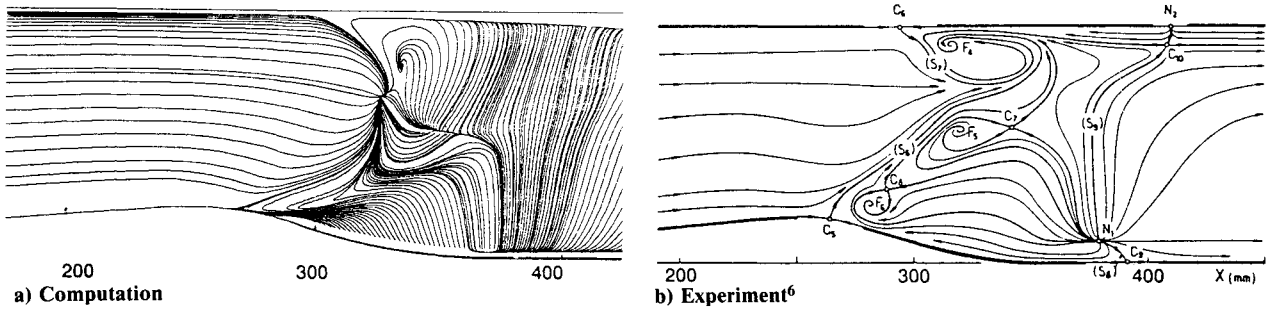

Fig. 17 Skin-friction lines on side wall A.

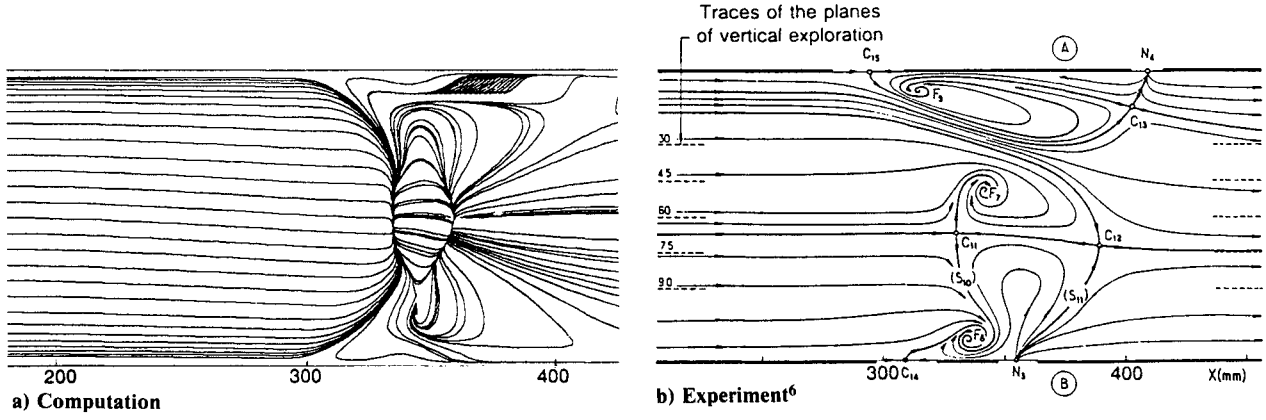

Fig. 18 Skin-friction lines on the upper wall.

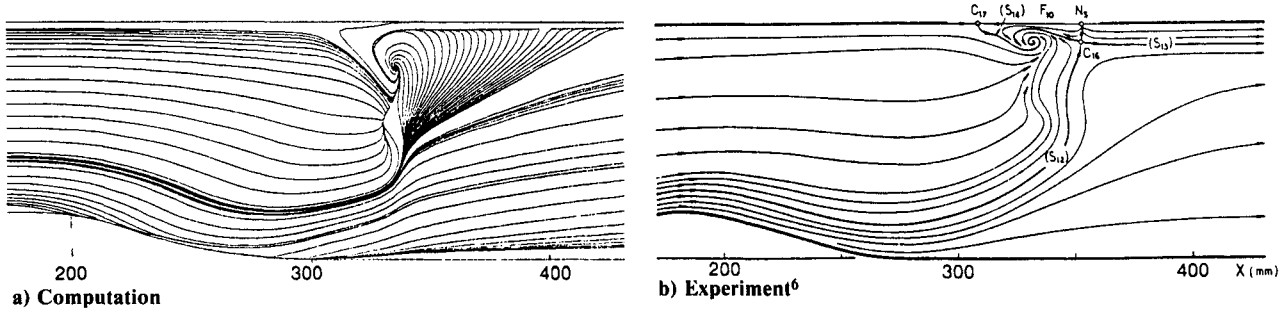

Fig. 19 Skin-friction lines on side wall B.

nent of the velocity is far greater near the lower wall than in the remaining part of the flow. In the plane $x = 300$ mm (see Fig. 14), the flow near the hump is greatly modified due to the interaction effect, and a vortex appears in the corner formed by the lower wall and wall A. Farther downstream (at $x = 340$ mm in Fig. 15), the extent of this vortex increases; near the upper wall, the transverse component intensity becomes far more important, and a vortex appears in each of the corners formed by the upper wall and the two lateral walls.

The surface patterns obtained by the skin-friction lines in the calculation and the viscous coating technique in the experiment provide valuable help in understanding the structure of a complex three-dimensional flow. Figures 16–19 show a comparison between the "postulated" experimental skin-friction lines[6] and the computed skin-friction lines on the four walls. The experimental skin-friction lines are said to be postulated

because they have been obtained from an interpretation of the viscous coating visualizations in light of topological laws involving the numbers of singular points classified as nodes, saddles, and foci. Agreement between computation and experiment is satisfactory on the side walls A and B (see Figs. 17 and 19) where the main features observed in the experiment are qualitatively well predicted by the computation. On the other hand, there are important discrepancies on the lower wall (see Fig. 16) where the computed structure is much simpler than the experimental one, and on the upper wall (see Fig. 18) where the numerical results are difficult to interpret. These discrepancies could probably be reduced by better grid resolution and turbulence modeling. However, a slightly different shock location between computation and experiment can also explain the skin-friction field disagreement since the flow structure has been found to be very sensitive to the shock location both in the computation and in the experiment, especially on the lower wall.

Concluding Remarks

A shock wave boundary-layer interaction has been simulated by numerically solving the Navier-Stokes equations. The results obtained in a mesh containing about 600,000 points and with a simple algebraic turbulence model are satisfactory since the calculation correctly represents some interesting features of the experimental flowfield. However, this is only a preliminary numerical investigation of a complex three-dimensional turbulent flowfield, and some important discrepancies between computation and experiment still exist. Further study is needed to explain and reduce the discrepancies. The two key issues that would improve the numerical results are certainly a better mesh resolution and a more sophisticated turbulence modeling.

Acknowledgments

The authors would like to thank J. Délery and his group for the definition of a very interesting test case for three-dimensional Navier-Stokes solvers, for having transmitted the experimental data, and for their help in the analysis of the numerical results. The authors would also like to acknowledge financial support from the "Direction des Recherches, Etudes et Techniques" (French Ministry of Defense).

References

[1]Cambier, L., and Délery, J., "Study of Turbulence Modeling in Transonic Shock Wave-Boundary Layer Interaction," *Proceedings of the 3rd International Conference on Numerical Methods in Laminar and Turbulent Flows,* edited by C. Taylor, J. A. Johnson, and W. R. Smith, Pineridge, Swansea, United Kingdom, Aug. 1983, pp. 198-209.

[2]Escande, B., and Cambier, L., "Turbulence Modeling in Transonic Interactions", *Proceedings of the IUTAM Symposium on Turbulent Shear-Layer/Shock-Wave Interactions,* Palaiseau, France, *Turbulent Shear-Layer/Shock-Wave Interactions,* edited by J. Délery, Springer-Verlag, 1986-ONERA TP No. 1985-128, 1985.

[3]Délery, J., "Investigation of Strong Shock Turbulent Boundary Layer Interaction in 2-D Transonic Flows with Emphasis on Turbulence Phenomena," *AIAA Journal,* Vol. 21, Feb. 1983, pp. 180-185.

[4]Vuillot, A. M., "A Multi-Domain 3D Euler Solver for Flows in Turbomachines," *Proceedings of the 9th ISABE Symposium,* edited by F. S. Billig, AIAA, Washington, D.C., Sept. 1989.

[5]Cambier, L., Couaillier, V., and Veuillot, J. P., "Numerical Solution of the Navier-Stokes Equations by a Multigrid Method," *La Recherche Aérospatiale,* No. 1988-2, March 1988, pp. 23-42 (English edition).

[6]Benay, R., Délery, J., and Pot, T., "Experimental Analysis of the Flow through a Three-Dimensional Transonic Channel," *Proceedings of the Propulsion and Energetics 68th (B) Specialists's Meeting,* Munich, AGARD CP No. 401 and *La Recherche Aérospatiale* No. 1986-6, Office National d'Etudes et de Recherches Aérospatiales, Châtillon, France, Sept. 1986, pp. 11-26 (English edition).

[7]Michel, R., Quémard, C., and Durant, R., "Application d'un schéma de longueur de mélange à l'étude des couches limites turbulentes d'équilibre," Office National d'Etudes et de Recherches Aérospatiales, Châtillon, France, NT No. 154, 1969.

[8]Buleev, N. I., "Theoretical Model of the Mechanism of Turbulent Exchange in Fluid Flows," *Teploperedacha,* Moscow, USSR, 1962, pp. 64-98, and *AERE Translation 957,* Atomic Energy Research Establishment, Harwell, England, 1963.

[9]Hung, C. M., and MacCormack, R. W., "Numerical Solution of Three-Dimensional Shock Wave and Turbulent Boundary Layer Interaction," *AIAA Journal,* Vol. 16, Oct. 1978, pp. 1090-1096.

[10]Thommen, H. U., "Numerical Integration of the Navier-Stokes Equations," *Zeitschrift für Angewandte Mathematic and Physik,* Vol. 17, 1966, pp. 369-384.

[11]Ni, R. H., "A Multigrid Scheme for Solving the Euler Equations," *AIAA Journal,* Vol. 20, Nov. 1982, pp. 1565-1571.

[12]Couaillier, V., "Solution of the Euler Equations: Explicit Scheme Acceleration by a Multigrid Method," *Proceedings of the 2nd European Conference on Multigrid Methods,* edited by U. Trottenberg and W. Hackbush, Gesellschaft für Mathematik und Datenverbarbeitung, Sankt Augustin, Germany, ONERA TP No. 1985-129, Oct. 1985.

[13]Couaillier, V., "Multigrid Method for Solving Euler and Navier-Stokes Equations in Two and Three Dimensions," *Proceedings of the 8th GAMM Conference on Numerical Methods in Fluid Mechanics, Notes on Numerical Fluid Mechanics,* Vol. No. 29, edited by P. Wesseling, Vieweg, Braunschweig, Germany.

[14]Couaillier, V., and Peyret, R., "Theoretical and Numerical Study of Ni's Multigrid Method," *La Recherche Aérospatiale,* Office National d'Etudes et de Recherches Aérospatiales, Châtillon, France, No. 1985-5, pp. 9-24 (English edition).

[15]Viviand, H., and Veuillot, J. P., "Méthodes pseudo-instationnaires pour le calcul d'écoulements transsoniques," Office National d'Etudes et de Recherches Aérospatiales, Châtillon, France, No. 1978-4 (English translation, ESA TT 561).